Available online at www.sciencedirect.com
SCIENCE DIRECT
Journal of Nuclear Materials 352 (2006) 341–348
journal of nuclear materials
www.elsevier.com/locate/jnucmat

Sintering behaviour and microstructures of carbides and nitrides for the inert matrix fuel by spark plasma sintering

Ho Jin Ryu [a,*], Young Woo Lee [a], Seung Il Cha [b], Soon Hyung Hong [b]

[a] Dry Process Fuel Technology Development Division, Korea Atomic Energy Research Institute, 150, Deokjin-dong, Yuseong-gu, Daejeon 305-353, South Korea
[b] Department of Material Science and Engineering, Korea Advanced Institute of Science and Technology, 373-1, Guseong-dong, Yuseong-gu, Daejeon 305-701, South Korea

Abstract

Zirconium carbide, titanium carbide, zirconium nitride and titanium nitride, which are promising candidates for the ceramic matrix of inert matrix fuel (IMF) to transmute long-lived actinides were sintered using the spark plasma sintering (SPS) technique. Dy_2O_3(20 wt%) was added as a surrogate for Am_2O_3 and the sintering behaviours of Dy_2O_3 dispersed carbide or nitride matrix composites were compared with that of the matrix. The spark plasma sintering conditions consisted of a rapid heating rate of 75 K min^{-1} and a very short holding time of 1–4 min at maximum temperatures ranging from 1773 to 2000 K. Dy_2O_3 dispersed carbides and nitrides with about 80% of theoretical density were obtained by spark plasma sintering with a rapid heating rate and a short dwelling time. When Dy_2O_3 was added to the matrix, the shrinkage of the carbide or of nitride composites was initiated from a lower temperature than its matrix material during the heating stage. In the case of TiC and TiN, microstructural observation exhibited that Ti is soluble in dysprosium oxide and densification is enhanced around the oxide phase.

1. Introduction

Inert matrix fuels (IMF) for transmutation of transuranium elements are proposed to reduce the radiotoxicity of spent fuels without producing new actinides. If suitable material systems for the IMF are developed successfully, IMF can be a promising option for the back-end fuel cycle for the transmutation of surplus plutonium and minor actinides (MA). The concept of transmutation of americium in the inert matrix was tested by the Experimental Feasibility of Targets for Transmutation (EFTTRA) project [1,2]. There are many requirements for the material properties of candidate IMF matrices such as high melting point, good thermal conductivity, and irradiation stability.

Although much experimental work have been being carried out for yttria stabilized zirconia (YSZ), magnesium oxide and spinel ($MgAl_2O_4$), carbides and nitrides such as ZrC, TiC, ZrN, and TiN have been considered as promising candidates for IMF recently. ZrC has been investigated as a diffusion barrier coating material for the coated particle fuel of high temperature gas cooled reactors

* Corresponding author. Tel.: +82 42 868 8845; fax: +82 42 868 8824.
E-mail address: hjyru@kaeri.re.kr (H.J. Ryu).

0022-3115/$ - see front matter © 2006 Published by Elsevier B.V.
doi:10.1016/j.jnucmat.2006.02.089

(HTGR) [3]. TiC and TiN are considered as inert matrices for dispersion fuel of the gas fast reactor (GFR) system [4,5]. ZrN will be irradiation-tested as a candidate for IMF in the collaboration on nitride fuel irradiation and modeling (CONFIRM) [6]. Streit et al. reported the fabrication results of (Pu,Zr)N as inert matrix fuel for accelerator driven systems (ADS) or fast reactors (FR) by using the direct coagulation casting, sol–gel, and carbothermic reduction [7]. At the Japan Atomic Energy Research Institute (JAERI), nitride matrix fuels such as (Pu,Zr)N and PuN + TiN were prepared by carbothermic reduction for an irradiation test [8].

Recently, the spark plasma sintering (SPS) technique, which is a rapid sintering process using the pulsed electric current, has been used for densification of advanced ceramic materials with low sinterability [9]. Kuwahara et al. [10] showed that fully dense TiN could be fabricated without binder and additive by the spark plasma sintering. Nanocrystalline TiN powder was successfully sintered by using spark plasma sintering compared to pressureless sintering, hot pressing and gas pressure sintering [11,12]. Adachi et al. [13] prepared a ZrN pellet for the inert matrix of an ADS target by spark plasma sintering to measure the thermal and electrical properties.

Consequently spark plasma sintering is proposed as an effective consolidation method for the dispersion type IMF composites which adopt strong covalent bonding ceramic matrices. Whereas spark plasma sintering of monolithic carbides and nitrides was investigated actively, spark plasma sintering of minor actinide dispersed carbides and nitrides were not reported yet. In this study, sintering behaviour of simulated MA oxide i.e. Dy_2O_3 dispersed carbides and nitrides for IMF is monitored and their microstructures were characterised after spark plasma sintering.

2. Experimental procedures

Commercial powders of zirconium carbide, titanium carbide, zirconium nitride and titanium nitride were supplied from Sigma–Aldrich Co. Dysprosia (Dy_2O_3) powder was selected as a surrogate for Am_2O_3 and also supplied from Sigma–Aldrich Co. [14]. After blending of 20 wt% Dy_2O_3 powder and matrix powder in a turbular mixer, the mixed powder was compacted in a cylindrical graphite die with an inner diameter of 10 mm. A spark plasma sintering system (Sumitomo Coal and Mining, Co., Dr. Sinter SPS-515S) was used for the sintering of each matrix powder (dispersed carbides or nitrides powders) with Dy_2O_3. In spark plasma sintering system, cylindrical graphite die and punches were electrically heated as shown in Fig. 1. Carbon felt covering was used for the thermal insulation of the die and non-contact temperature measurement of a hole in the graphite die near the sintered compact was provided by an optical pyrometer temperature sensor. The sintering temperature varied from 1773 to 2000 K, the heating rate was 75 K min^{-1} and the holding time at the maximum temperature ranged from 1 to 4 min. Vacuum atmosphere of about 3 Pa and compressive pressure of 30 MPa were maintained during the spark plasma sintering. For the sintering of carbides, 0.2 wt% of graphite was added to reduce the oxide surface during sinter-

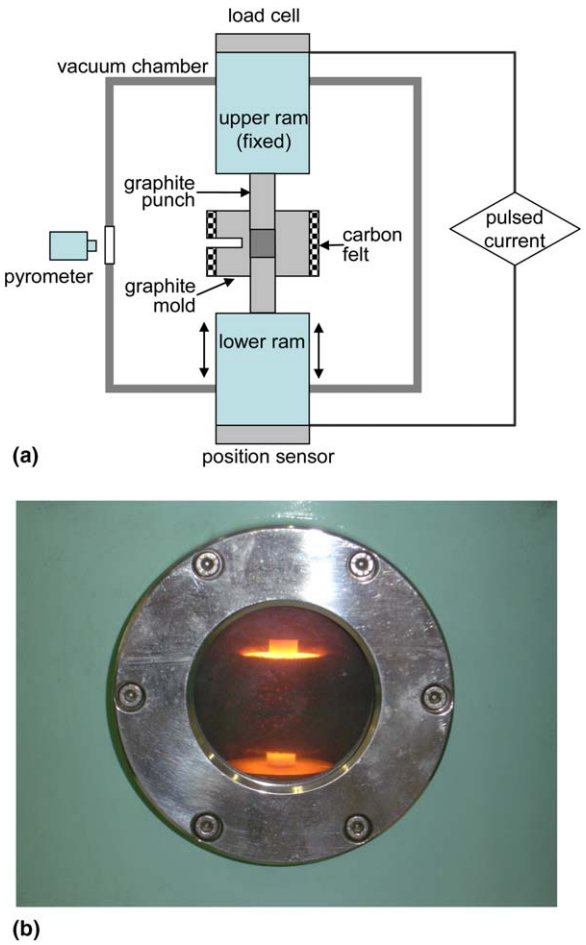

Fig. 1. (a) Experimental set-up of the spark plasma sintering system and (b) a photograph of a graphite mold and punches during sintering of an inert matrix fuel.

ing. Axial displacement of the lower punch which presses the powder compact upward is monitored by a position sensor in the spark plasma sintering system. The relative density of the sintered pellets was measured using the water immersion method. The crystal structures of sintered pellets were evaluated by X-ray powder diffraction. The microstructure of sintered pellets was observed by field

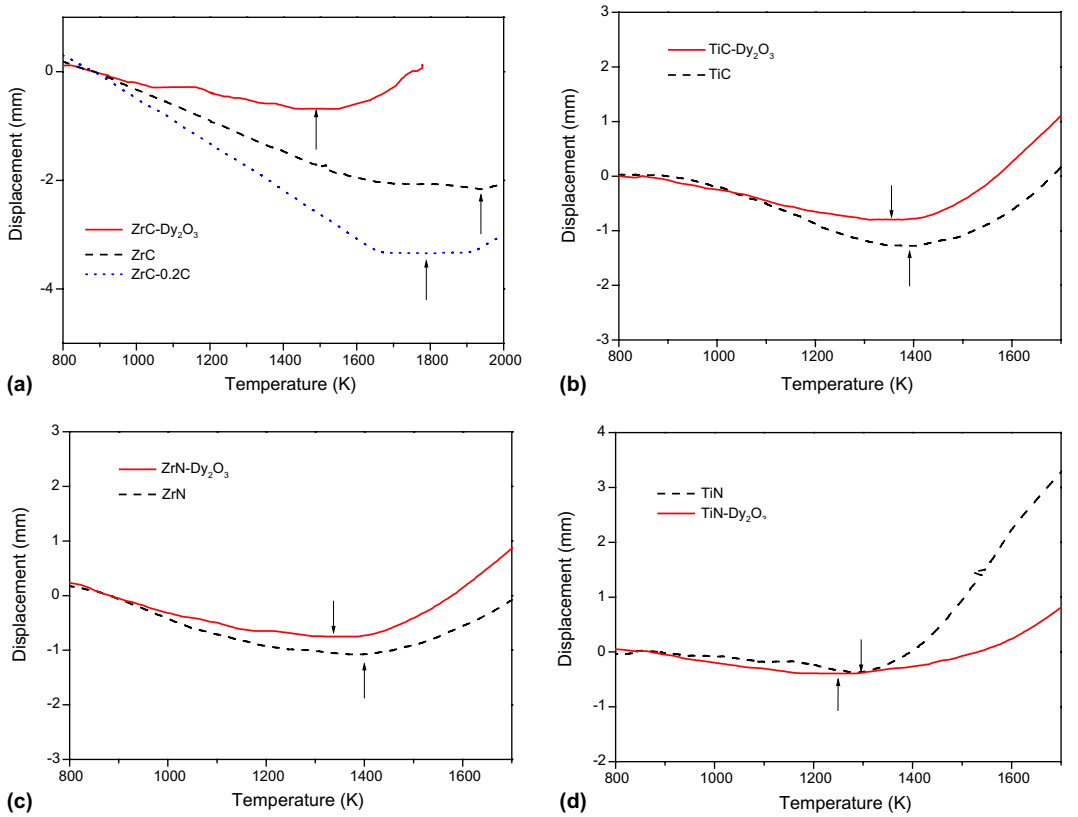

Fig. 2. Shrinkage behavior of inert matrices and their Dy_2O_3 dispersed composites during the spark plasma sintering: (a) ZrC, (b) TiC, (c) ZrN and (d) TiN. (Arrows indicate the minimum position of each curve.)

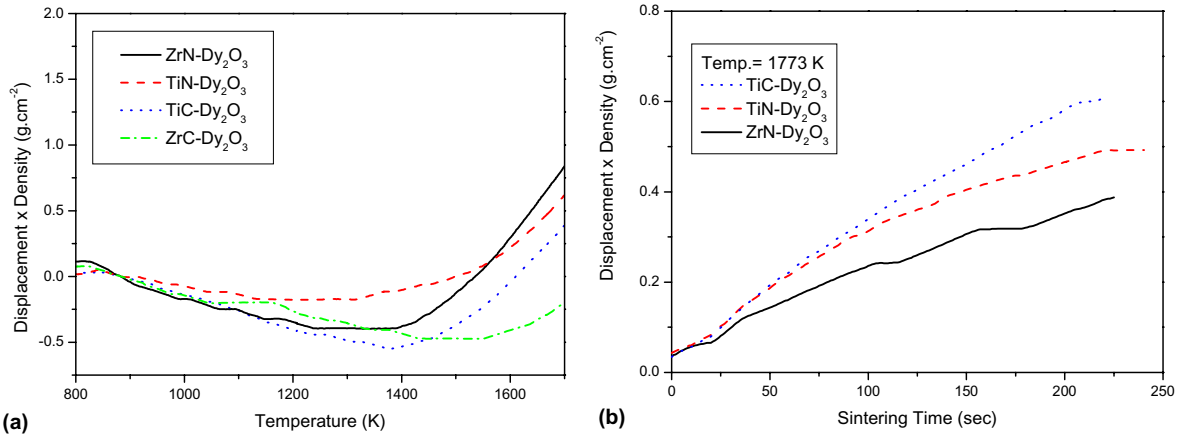

Fig. 3. Sintering behavior comparison for each system: (a) with increasing temperature up to 1773 K at a heating rate of 75 K min^{-1} and (b) with increasing dwelling time at 1773 K.

emission scanning electron microscopy (FE-SEM) and energy dispersive X-ray spectroscopy (EDS) was used for compositional analysis.

3. Results and discussion

Spark plasma sintering is also known as pulsed electric currents sintering (PECS) or field assisted sintering. The enhanced sintering by spark plasma sintering technique the particles to be sintered is attributed to the electric discharge or spark plasma between [15]. The principal advantages of the spark plasma sintering over conventional hot pressing and hot isostatic pressing (HIP) are lower sintering temperatures, rapid heating rates and short dwell times for hard-to-sinter ceramic materials with strong covalent bonds.

Fig. 2 shows the axial shrinkage behaviour of the sintered pellets obtained from the axial displacement data. During the heating, the position of the lower punch moves down due to thermal expansion of the powder compact until sintering between the particles takes place. When sintering of the powder is initiated, the downward curve changes its slope to an upward direction according to the densification rate of the powder compact. The minimum position of the displacement curve is a temperature where the contribution of sintering shrinkage begins to increase effectively. When we compare the shrinkage behaviour of monolithic carbides and nitrides with that of Dy_2O_3 containing inert matrix composites, it is found that the sintering onset temperature is

Table 1
Density of sintered matrix and composite for each system

System	Measured density (g cm^{-3})	Theoretical density (g cm^{-3})	Relative density (%)
ZrC	4.27	6.73	63
ZrC–Dy_2O_3	4.69	6.92	68
TiC	3.63	4.90	74
TiC–Dy_2O_3	4.19	5.29	79
ZrN	4.63	7.09	65
ZrN–Dy_2O_3	5.34	7.22	74
TiN	4.29	5.22	82
TiN–Dy_2O_3	4.36	5.59	78

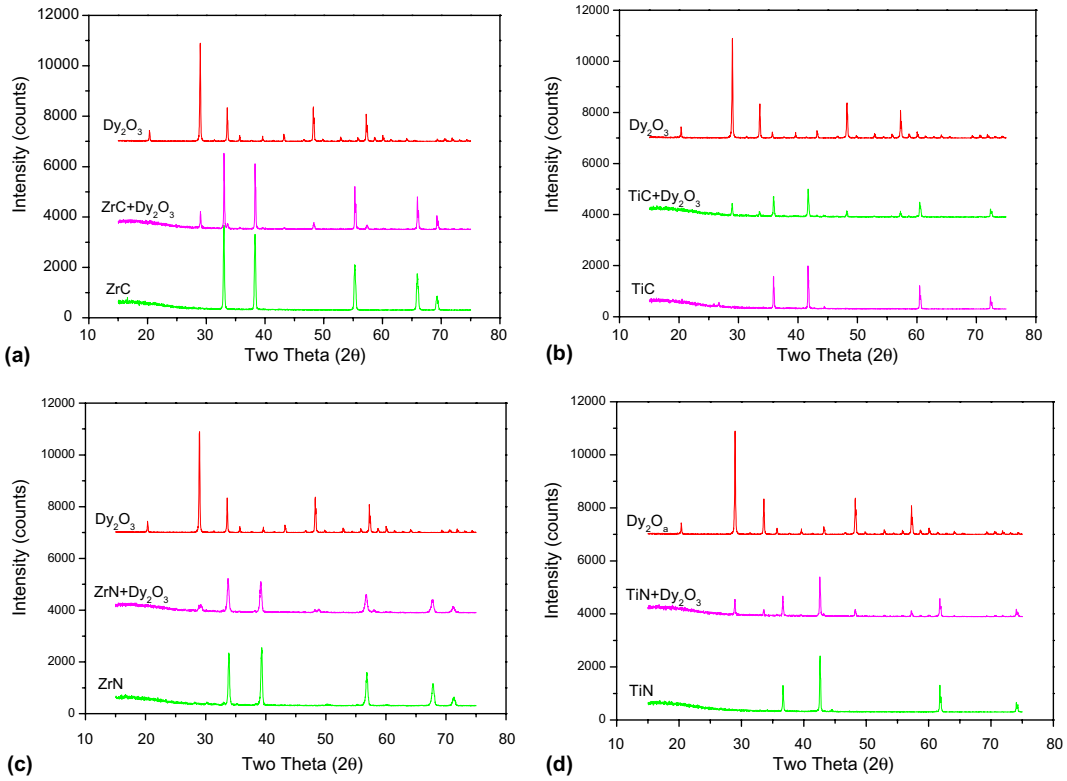

Fig. 4. XRD pattern of sintered pellet: (a) ZrC and ZrC–Dy_2O_3, (a) TiC and TiC–Dy_2O_3, (c) ZrN and ZrN–Dy_2O_3 and (d) TiN and TiN–Dy_2O_3.

lower for the Dy_2O_3 containing composites than its monolithic matrices during the heating stage. Sintering of carbides and nitrides was facilitated by the addition of Dy_2O_3. The enhanced sintering of Dy_2O_3 added carbides and nitrides can be attributed to the removal of the oxide surface and enhanced diffusion compared to the similar results of many researchers as follows. Sakai and Iwata [16] reported that the self-diffusion coefficient of AlN increases with increasing oxygen content because cation vacancies are introduced in AlN crystals by oxygen doping. Zhou et al. [17] explained that Y_2O_3 or La_2O_3 additives can serve as oxygen catcher by reacting with oxide impurity both on the surface of SiC particles and within the SiC lattice. Levin et al. [18] showed that TiO_2 is reduced by carbon originates in B_4C when it is added for B_4C sintering. The resulting improved sintering behaviour of B_4C is attributed to the enhanced mass transport processes that takes place in substoichiometric B_4C.

Although Khor et al. [19] reported that the addition of Sm_2O_3 as a sintering aid improves the sintered density of AlN because the use of Sm_2O_3 leads to formation of a liquid phase in the Sm_2O_3–Al_2O_3–AlN system. This liquid phase improves mass transport during sintering. The sintering onset temperature observed in this experiment is thought to be far below the liquid forming temperature and an abrupt change in axial displacement was not observed.

When a small amount of graphite (0.2 wt%) was added to ZrC, the sintering onset temperature became lower than pure ZrC without graphite as shown in Fig. 2(a). The role of graphite is considered to reduce the surface oxide layer, which inhibits sound contact between the carbide particles.

The sintering behaviour of each system was compared by normalizing the z-axis displacement curve. The theoretical density of each system was calculated by the rule-of-mixtures and the shrinkage of each system was then obtained by multiplying the

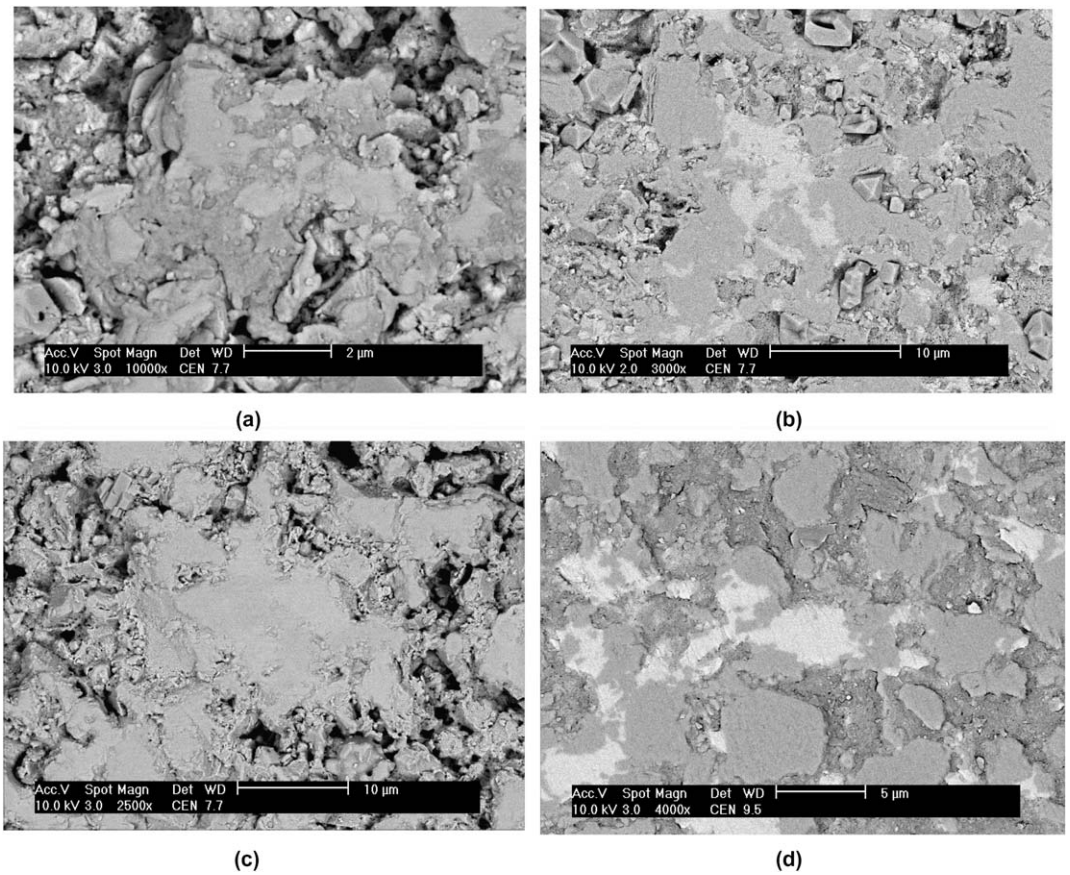

Fig. 5. Scanning electron micrographs of (a) Dy_2O_3 added ZrC, (b) Dy_2O_3 added TiC, (c) Dy_2O_3 added ZrN, and (d) Dy_2O_3 added TiN. (Brighter phase is oxide in backscattered electron images.)

theoretical density by the axial displacement. Fig. 3(a) shows that the sintering of TiN matrix composite starts at the lowest temperature while the ZrC matrix composite begins to sinter at the highest temperature among the four systems. When the shrinkage of each system was compared at a constant temperature (1773 K) with increasing time see Fig. 3(b), it is clear that TiC matrix composite shows the most rapid densification rate.

Measured densities of sintered pellets were represented as shown in Table 1. Theoretical density for each dysprosium oxide added composite was calculated by the rule-of-mixtures assumption. The addition of Dy_2O_3 resulted in an increase of the relative

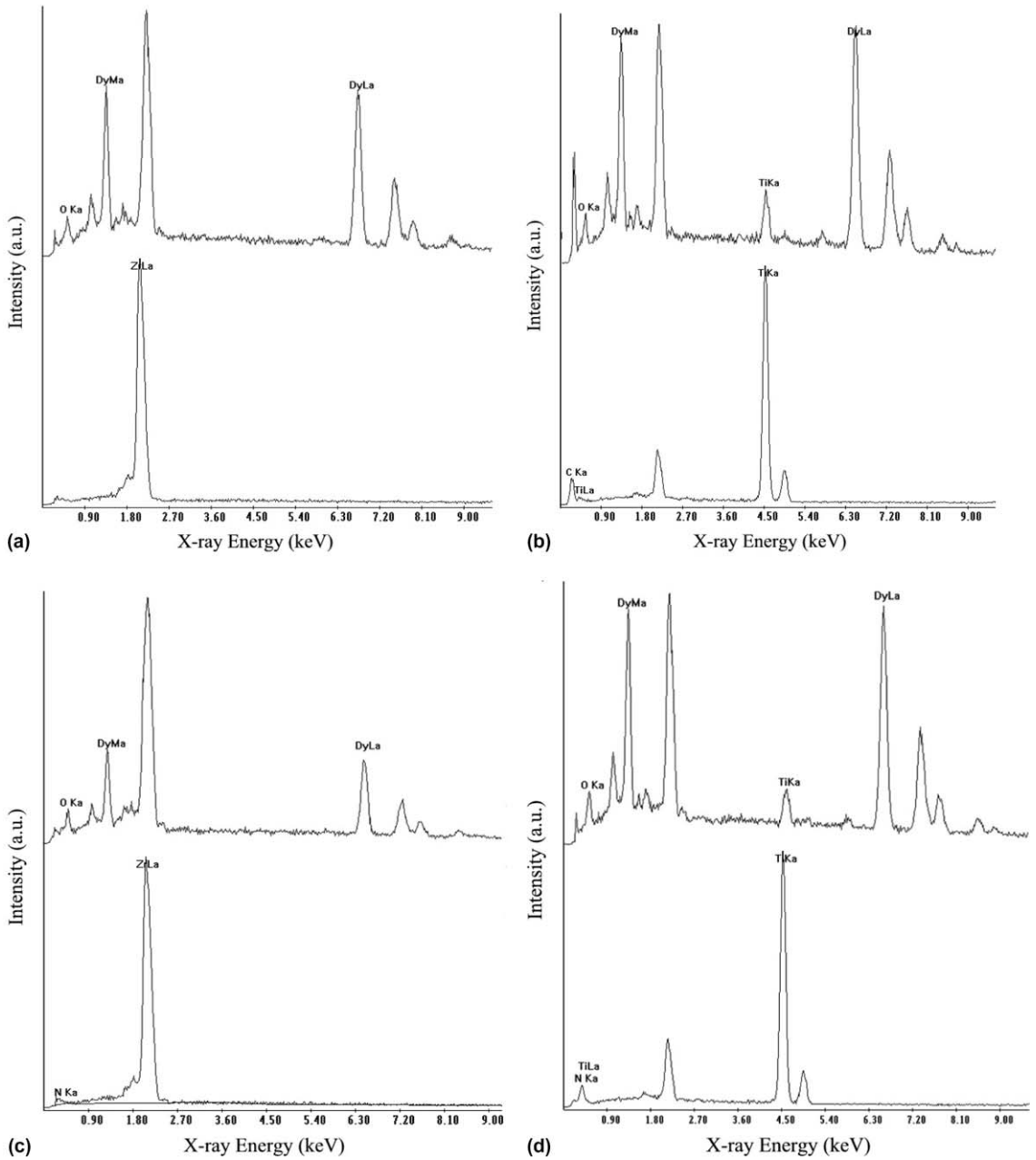

Fig. 6. Energy dispersive X-ray spectroscopy of (a) Dy_2O_3 added ZrC, (b) Dy_2O_3 added TiC, (c) Dy_2O_3 added ZrN, and (d) Dy_2O_3 added TiN. Lower spectrum represents matrix phase and upper spectrum represents oxide phase in each system.

density in all matrices except in the TiN matrix composite. Spark plasma sintering conditions such as sintering temperatures and dwelling times employed in this experiment are thought to be insufficient to activate diffusion of mass because the melting point of ZrC is the highest (3523 K) compared to other matrices. The relative density of carbide and nitride pellets can be increased up to 98% by applying mechanical milling of powder before spark plasma sintering [20]. The effect of mechanical milling is attributed mainly to the particle size refinement and enhanced surface area [21]. Therefore the density of Dy_2O_3 dispersed composite can be controlled by varying the mechanical milling conditions.

The crystal structures and lattice parameters of ZrC, TiC, ZrN, TiN, and their Dy_2O_3 containing composites were obtained by X-ray powder diffraction of the sintered pellets as shown in Fig. 4. Dy_2O_3 dispersed carbides and nitrides showed a mixed pattern from the original phase and Dy_2O_3. New peaks for interaction phase or peak shift due to solid solution were not observed in the X-ray diffraction patterns. This means that the probable interaction between Dy_2O_3 and matrix phase is not so active to be detected by X-ray diffraction. Consequently, Dy_2O_3 added carbides and nitrides form dispersion type IMF systems that have some advantages on irradiation performances, because radiation damages can severely degrade the matrix properties in a solid solution systems such as (Am,Zr)N [22].

Further investigations using neutron diffraction are required to explain the presence of minor phase or slight shift in peak position. The lattice parameter of sintered carbides and nitrides showed good agreement with the lattice parameters reported in the literature. For example, the lattice parameter of ZrN prepared by the spark plasma sintering was measured as 0.4581 nm and it is located within 0.1% error range compared with the theoretical value (0.4578 nm).

When sintered microstructures were observed by scanning electron microscopy as shown in Fig. 5, oxide phases in zirconium carbide and zirconium nitride matrix composites were found to be isolated in the porous area. On the other hand, oxide phases in titanium carbide and titanium nitride matrix composites were located in the highly densified area surrounded by the matrix phase.

Chemical composition analysis by energy dispersive X-ray spectroscopy shows a different behavior of Zr and Ti in the oxide phase in their composites. As shown in Fig. 6(a) and (c), Zr was not detected in the oxide phase of the ZrC and ZrN matrix composites, whereas 6.0–9.0 at.% of Ti exist in the oxide phase of the TiC and TiN as shown in Fig. 6(b) and (d). Dy is not detected both in the carbide and nitride phases. Ti is known to be soluble in Dy_2O_3 and there exist two stable compounds such as Dy_2TiO_5 and $Dy_2Ti_2O_7$ that are used as an absorber material for control rods in the VVER type Russian reactors [23]. Considering the atomic fraction of Ti in the oxide and the result of the X-ray diffraction study, the dysprosium titanate phase is not thought to be formed. It is found that sintering of the matrix phase located around the oxide was locally enhanced as it can be seen in Fig. 5, when the matrix phase has some solubility in dispersed oxide.

4. Conclusions

Dy_2O_3 dispersed ZrC, TiC, ZrN and TiN matrix composites were obtained by spark plasma sintering with a rapid heating rate and a short dwelling time. When Dy_2O_3 is added to the matrix, a shrinkage of the carbide or nitride composite was initiated at a lower temperature than the pure matrix material during the heating stage. X-ray diffraction showed that Dy_2O_3 and each matrix phase maintain their original nature after a sintering. Microstructural observation showed that Ti has some solubility for Dy_2O_3 and a locally enhanced sintering occurred around the oxide phase in the TiC or TiN matrix composites. This study proposes that minor actinides as an oxide form can be dispersed in carbide or nitride matrix to fabricate oxide-dispersed IMF pellets. Further study using americium oxide will be more valuable to verify the performance of the oxide dispersed IMF.

Acknowledgement

This work was supported by the National Nuclear R&D Program of Ministry of Science and Technology (MOST) of Korea.

References

[1] J.-F. Babelot, R. Conrad, R.J.M. Konings, G. Mühling, M. Salvatores, G. Vambenepe, J. Nucl. Mater. 271–273 (1999) 606.
[2] R.J.M. Konings, K. Bakker, J.G. Boshoven, H. Hein, M.E. Huntelaar, R.R. Van der Laan, J. Nucl. Mater. 274 (1999) 84.

[3] T. Ogawa, K. Fukuda, S. Kashimura, T. Tobita, F. Kobayashi, S. Kado, H. Miyanishi, I. Takahashi, T. Kikuchi, J. Am. Ceram. Soc. 75 (1992) 2985.
[4] S. Bourg, F. Péron, J. Lacquement, in: Proceedings of ATALANTE 2004, Advances for future nuclear fuel cycles, Nîmes, France, 21–24 June, 2004.
[5] E.A. Hoffman, T.A. Taiwo, W.S. Yang, M. Fatone, in: Proceedings of 7th Information Exchange Meeting on Actinide and Fission Product Partitioning and Transmutation, Jeju, Republic of Korea, 14–16 October, 2002.
[6] M. Streit, F. Ingold, J. Europ. Ceram. Soc. 25 (2005) 2687.
[7] M. Streit, F. Ingold, M. Pouchon, L.J. Gauckler, J.-P. Ottaviani, J. Nucl. Mater. 319 (2003) 51.
[8] K. Minato, M. Akabori, M. Takano, Y. Arai, K. Nakajima, A. Itoh, T. Ogawa, J. Nucl. Mater. 320 (2003) 18.
[9] M. Tokita, in: Proceedings of International Symposium On Microwave, Plasma and Thermomechanical Processing of Advanced Materials, 1977, p. 69.
[10] H. Kuwahara, N. Mazaki, M. Takahashi, T. Watanabe, X. Yang, T. Aizawa, Mater. Sci. Eng. A 319–321 (2001) 687.
[11] J.R. Groza, J.P. Curtis, M. Kramer, J. Am. Ceram. Soc. 83 (2000) 1281.
[12] P. Angerer, L.G. Yu, K.A. Khor, G. Korb, I. Zalite, J. Europ. Ceram. Soc. 25 (2005) 1919.
[13] J. Adachi, K. Kurosaki, M. Uno, S. Yamanaka, J. Alloys Compd. 399 (2005) 242.
[14] T. Ogawa, K. Minato, Pure Appl. Chem. 73 (2001) 799.
[15] M. Tokita, J. Soc. Powder Tech. Jpn. 30 (1993) 790.
[16] T. Sakai, M. Iwata, J. Mater. Sci. 12 (1977) 1659.
[17] Y. Zhou, K. Hirao, K. Watari, Y. Yamauchi, S. Kanzaki, J. Europ. Ceram. Soc. 24 (2004) 265.
[18] L. Levin, N. Frage, M.P. Dariel, Metall. Mater. Trans. A 30 (1999) 3201.
[19] K.A. Khora, L.G. Yua, Y. Murakoshi, J. Europ. Ceram. Soc. 25 (2005) 1057.
[20] J.H. Won, K.H. Kim, J.H. Chae, K.B. Shim, J. Ceram. Process. Res. 3 (2002) 166.
[21] S.H. Na, S.H. Kim, Y.W. Lee, D.S. Sohn, J. Kor. Nucl. Soc. 34 (2002) 60.
[22] N. Chauvin, R.J.M. Konings, Hj. Matzke, J. Nucl. Mater. 274 (1999) 105.
[23] V.D. Risovany, E.E. Varlashova, D.N. Suslov, J. Nucl. Mater. 281 (2000) 84.